IEEE Photonics Journal
An IEEE Photonics Society Publication

Open Access

Low-PAPR Asymmetrically Clipped Optical OFDM for Intensity-Modulation/Direct-Detection Systems

Volume 7, Number 3, June 2015

Ji Zhou
Yaojun Qiao, Member, IEEE

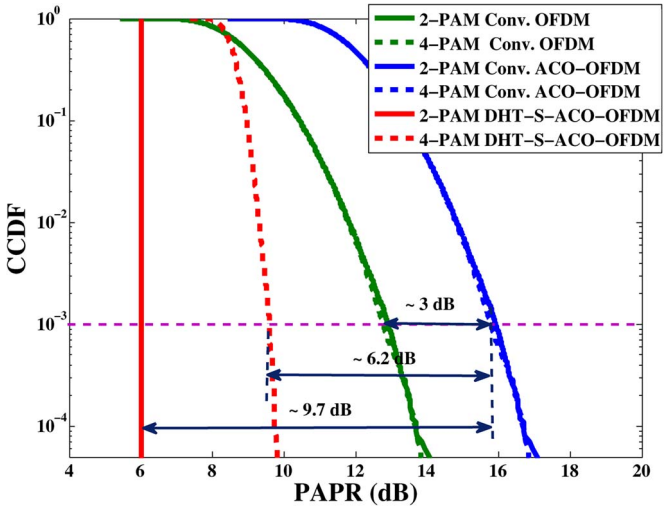

DOI: 10.1109/JPHOT.2015.2430843
1943-0655 © 2015 IEEE

IEEE photonics SOCIETY

IEEE

Low-PAPR Asymmetrically Clipped Optical OFDM for Intensity-Modulation/Direct-Detection Systems

Ji Zhou and Yaojun Qiao, *Member, IEEE*

State Key Laboratory of Information Photonics and Optical Communications, School of Information and Communication Engineering, Beijing University of Posts and Telecommunications (BUPT), Beijing 100876, China

DOI: 10.1109/JPHOT.2015.2430843

Manuscript received April 6, 2015; revised May 3, 2015; accepted May 4, 2015. Date of publication May 7, 2015; date of current version May 27, 2015. This work was supported in part by the National Natural Science Foundation of China under Grant 61271192, Grant 61427813, and Grant 61331010; by the National 863 Program of China under Grant 2013AA013401; and by the Postgraduate Innovation Fund of SICE, BUPT, 2015. Corresponding author: Y. Qiao (e-mail: qiao@bupt.edu.cn).

Abstract: In this paper, we propose a discrete Hartley transform (DHT)-spread technique for peak-to-average power ratio (PAPR) reduction in a DHT-based asymmetrically clipped optical orthogonal frequency-division multiplexing (ACO-OFDM) system. At the complementary cumulative distribution function of 10^{-3}, the PAPR values of our proposed scheme are about 9.7 and 6.2 dB lower than those of conventional DHT-based ACO-OFDM without DHT-spread technique for 2-pulse-amplitude modulation (2-PAM) and 4-PAM, respectively. The transmission experiment over a 100-km standard single-mode fiber had been realized to verify the feasibility of the proposed scheme. When the overall link rate was about 10 Gb/s, the proposed scheme had an approximately 7-dB improvement of received sensitivity at forward error correction limit compared with the conventional scheme. The proposed scheme has better transmission performance than the conventional scheme due to its low PAPR and effective equalization.

Index Terms: Discrete Hartley transform (DHT), DHT-spread technique, asymmetrically clipped optical orthogonal frequency-division multiplexing (ACO-OFDM), peak-to-average power ratio (PAPR) reduction, intensity-modulated/direct-detection (IM/DD) systems.

1. Introduction

As a multicarrier modulation technique, orthogonal frequency division multiplexing (OFDM) has been used in optical communication due to its high spectral efficiency and resistance to inter-symbol interference (ISI) [1]–[3]. Among the OFDM systems, intensity-modulated/direct-detection (IM/DD) OFDM system has been widely investigated in the cost-sensitive, short-range, and high-speed optical communications, such as indoor optical wireless communication, discrete multi-tone (DMT) systems and passive optical networks (PONs) [4]–[6].

As a popular IM/DD system, asymmetrically clipping optical OFDM (ACO-OFDM) has been extensively researched [8]–[10]. ACO-OFDM has a good power efficiency and the same optimal design for all constellation sizes due to the nonuse of DC bias, which is attractive to IM/DD system [8]. Recently, ACO-OFDM based on discrete Hartley transform (DHT) has been proposed for IM/DD system [11], [12]. DHT is a real trigonometric transform. Different from DFT-based

ACO-OFDM, DHT-based ACO-OFDM does not need Hermitian symmetry (HS), and the same algorithm can be applied to the multiplexing and demultiplexing processes. When DFT and DHT have the same size, 2-pulse-amplitude modulation (2-PAM) (M-PAM)-modulated DHT-based ACO-OFDM transmits the same number of bits and has the same bit-error ratio (BER) performance as QPSK (M^2-QAM)-modulated DFT-based ACO-OFDM [11]–[13].

High peak-to-average power ratio (PAPR) is one of the major drawbacks of OFDM, which brings serious nonlinear distortion in both electronic and optical domain. Compared to OFDM without clipping operation, ACO-OFDM has a higher PAPR due to the same peak power but lower average power caused by clipping operation. Therefore, it is much more essential for ACO-OFDM to decrease PAPR. Among the PAPR reduction techniques, DFT-spread technique without any signal distortion and coding overhead has been widely studied [14]–[17]. To the best of our knowledge, the spread technique has not been investigated in DHT-based ACO-OFDM system.

In this paper, we propose a DHT-spread technique for PAPR reduction in DHT-based ACO-OFDM and analyze the performance of DHT-spread technique by both simulations and experiments. Different from DFT-spread technique, DHT-spread technique has the real output, making it more suitable for the DHT-based ACO-OFDM system. At the complementary cumulative distribution function (CCDF) of 10^{-3}, the PAPR values of our proposed scheme are about 9.7 dB and 6.2 dB lower than those of conventional DHT-based ACO-OFDM without DHT-spread technique for 2-PAM and 4-PAM, respectively. The transmission experiment over 100-km standard single mode fiber (SSMF) had been realized to verify the feasibility of the proposed scheme. When the overall link rate was about 10 Gb/s, the proposed scheme had an about 7-dB improvement of received sensitivity at forward error correction (FEC) limit compared to conventional scheme. The proposed scheme has better performance on equalization and nonlinear distortion mitigation than the conventional scheme.

2. Principle

The multiplexing/demultiplexing processes of the proposed OFDM scheme use the DHT algorithm. The N-point inverse DHT (IDHT) and DHT [13] are defined as

$$x_n = \frac{1}{\sqrt{N}} \sum_{k=0}^{N-1} X_k \mathrm{cas}\left(\frac{2\pi kn}{N}\right), \qquad X_k = \frac{1}{\sqrt{N}} \sum_{n=0}^{N-1} x_n \mathrm{cas}\left(\frac{2\pi kn}{N}\right) \tag{1}$$

where $\mathrm{cas}(.) = \cos(.) + \sin(.)$, n and k are from 0 to $N-1$, x_n is the time-domain OFDM sample, and X_k is the frequency-domain input sample. As shown in (1), DHT is a real trigonometric transform with a self-inverse property. Unlike the DFT-based IM/DD OFDM, DHT-based IM/DD OFDM does not need HS to generate real signal and the multiplexing and demultiplexing processes employ the same algorithm.

Next, if no otherwise specified, all the multiplexing/demultiplexing processes of OFDM mentioned below use the DHT algorithm.

The block diagram of DHT-spread ACO-OFDM (DHT-S-ACO-OFDM) for IM/DD system is depicted in Fig. 1. Unlike conventional ACO-OFDM, DHT-S-ACO-OFDM adds two L-point DHT modules in the transmitter and receiver as the red boxes show. At transmitter, the data sequences are sent to the real constellation mapper [PAM mapper] after serial-to-parallel operation. Then the generated M-PAM signals are sent to the L-point DHT to realize the DHT-spread operation. The output of L-point DHT $\boldsymbol{x}$ is defined as

$$x_m = \frac{1}{\sqrt{L}} \sum_{l=0}^{L-1} X_l \mathrm{cas}\left(\frac{2\pi lm}{L}\right) \tag{2}$$

where m is from 0 to $L-1$. x_m is assigned to odd positions of N-point DHT operation (i.e., $N = 2L$)

$$\boldsymbol{y} = [0, x_0, 0, x_1, \ldots, x_{L-1}]. \tag{3}$$

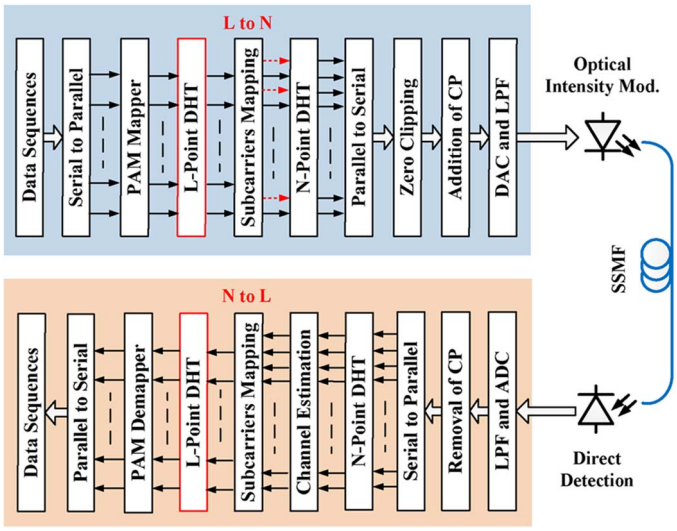

Fig. 1. Block diagram of DHT-spread ACO-OFDM for IM/DD system.

After N-point DHT operation, the generated OFDM, $\boldsymbol{Y}$, can be defined as

$$Y_i = \frac{1}{\sqrt{2L}} \sum_{h=0}^{2L-1} y_h \mathrm{cas}\left(\frac{2\pi hi}{2L}\right) = \frac{1}{\sqrt{2L}} \sum_{j=0}^{L-1} y_{2j+1} \mathrm{cas}\left(\frac{2\pi(2j+1)i}{2L}\right) \tag{4}$$

where i is from 0 to $N-1$.

As shown in (3), $y_{2j+1} = x_j$

$$\begin{aligned} Y_i &= \frac{1}{\sqrt{2L}} \sum_{j=0}^{L-1} x_j \mathrm{cas}\left(\frac{2\pi(2j+1)i}{2L}\right) \\ &= \frac{1}{\sqrt{2L}} \sum_{j=0}^{L-1} \frac{1}{\sqrt{L}} \sum_{l=0}^{L-1} X_l \mathrm{cas}\left(\frac{2\pi lj}{L}\right) * \mathrm{cas}\left(\frac{2\pi(2j+1)i}{2L}\right) \\ &= \frac{1}{\sqrt{2L}} \sum_{j=0}^{L-1} \sum_{l=0}^{L-1} X_l \left[\cos\left(\frac{2\pi(i-l)j - \pi i}{L}\right) + \sin\left(\frac{2\pi(i+l)j + \pi i}{L}\right)\right]. \end{aligned} \tag{5}$$

Therefore, we can get the output of N-point DHT $\boldsymbol{Y}$

$$Y_i = \begin{cases} \frac{1}{\sqrt{2}}\left[X_i \cos\left(\frac{\pi i}{L}\right) + X_{L-i} \sin\left(\frac{\pi i}{L}\right)\right], & 0 \le i \le L-1 \\ \frac{1}{\sqrt{2}}\left[X_{i-L} \cos\left(\frac{\pi i}{L}\right) + X_{2L-i} \sin\left(\frac{\pi i}{L}\right)\right], & L \le i \le 2L-1. \end{cases} \tag{6}$$

$\boldsymbol{Y}$ has the anti-symmetrical property (i.e. $Y_i = -Y_{i+L}, 0 \le i \le L-1$). The negative samples of $\boldsymbol{Y}$ can be forced to zero without any loss of information [7]. The DHT-S-ACO-OFDM, $\boldsymbol{C}$, can be obtained from $\boldsymbol{Y}$ by clipping operation,

$$C_i = \begin{cases} Y_i, & Y_i > 0 \\ 0, & Y_i \le 0 \end{cases} \tag{7}$$

where i is from 0 to $N-1$. After addition of cyclic prefix (CP), digital-to-analog conversion (DAC) and low-pass filter (LPF) modules, the transmitted signal is generated.

At receiver, the inverse operations of transmitter are realized to recover the data sequences, mainly including analog-to-digital conversion (ADC), removal of CP, N-point DHT, channel estimation, L-point DHT and PAM demapper.

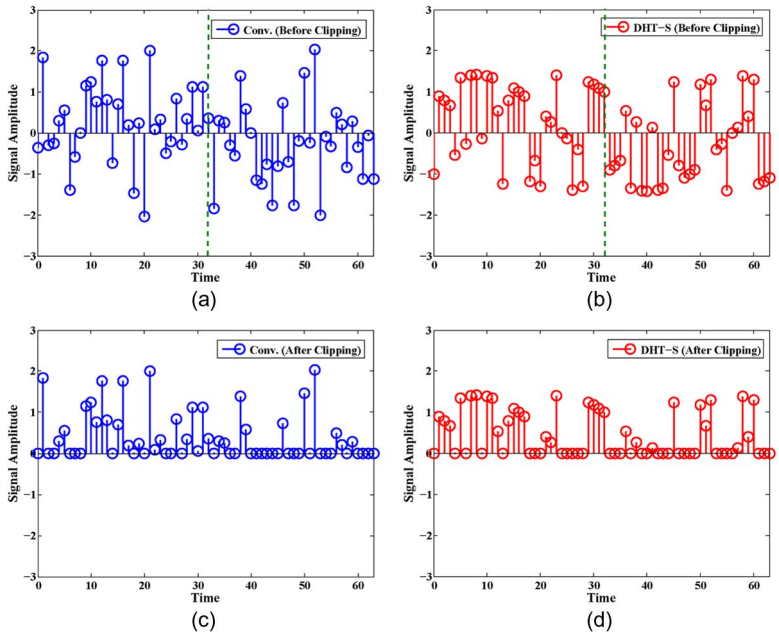

Fig. 2. (a) Anti-symmetry conventional OFDM symbol. (b) Anti-symmetry DHT-S-OFDM symbol. (c) Conventional ACO-OFDM symbol. (d) DHT-S-ACO-OFDM symbol. The N is equal to 64.

3. Simulation Results and Discussions

3.1. Time Domain Symbol

Fig. 2 shows time domain symbols before and after clipping operation in conventional ACO-OFDM and DHT-S-ACO-OFDM where N is set to 64. As shown in Fig. 2(a) and (b), the green dash line points out the position of the 32nd sample. Obviously, the symbols before clipping operation in conventional ACO-OFDM and DHT-S-ACO-OFDM systems are both anti-symmetry. The average power of the symbol after clipping operation is half that of the symbol before clipping operation. PAPR of the symbols after clipping operation are theoretically 3 dB higher than that of the symbols before clipping operation. Consequently, it is much more essential for ACO-OFDM to decrease the PAPR. We have set the symbols in Fig. 2(c) and (d) with the same average power, the symbol in Fig. 2(c) obviously has larger peak power than the symbol in Fig. 2(d). PAPR of DHT-S-ACO-OFDM should be lower than that of conventional ACO-OFDM.

3.2. CCDF Curves of PAPR

The PAPR, which is defined as the ratio between the maximum peak power and the average power of the discrete OFDM signal, can be expressed as

$$\mathrm{PAPR} = 10\log_{10}\left(\frac{\mathrm{Max}\left\{|S_i|^2\right\}}{E\left\{|S_i|^2\right\}}\right) \tag{8}$$

where S_i is OFDM signal, and $E\{.\}$ denotes the statistical expectation [18].

When 2-PAM is modulated in DHT-S-ACO-OFDM, by calculating (6) and (7), the maximum peak power and average power are equal to 1 and 1/4, respectively. Therefore, the PAPR can be calculated from (8) as

$$\mathrm{PAPR} = 10\log_{10}\left(\frac{\mathrm{Max}\left\{|C_i|^2\right\}}{E\left\{|C_i|^2\right\}}\right) = 10\log_{10}\left(\frac{1}{1/4}\right) = 6\ \mathrm{dB}. \tag{9}$$

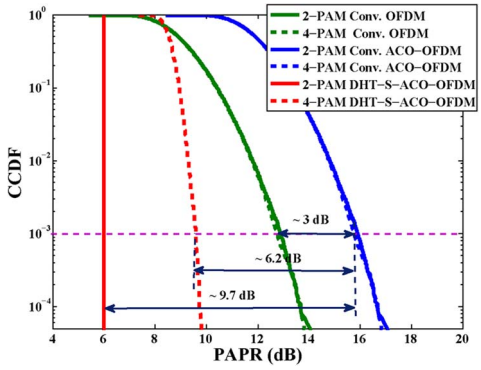

Fig. 3. Complementary cumulative distribution function (CCDF) curves of w/o clipping OFDM, conventional ACO-OFDM, and DHT-S-ACO-OFDM.

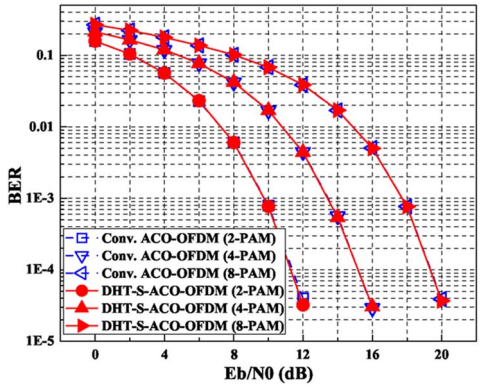

Fig. 4. Comparison of BER performance between conventional ACO-OFDM and DHT-S-ACO-OFDM in AWGN channel.

The CCDF is commonly used to evaluate the performance of PAPR reduction techniques. The CCDF of the PAPR denotes the probability that the PAPR of an OFDM symbol exceeds a threshold PAPR_0. We define the CCDF as

$$\mathrm{CCDF} = \mathrm{P}(\mathrm{PAPR} > \mathrm{PAPR}_0). \tag{10}$$

Fig. 3 reveals the CCDF curves of PAPR for w/o clipping OFDM, conventional ACO-OFDM, and DHT-S-ACO-OFDM. In the simulation for CCDF curves, the number of subcarriers is set to 256 and the number of symbols for the probability of 10^{-4} is set to 10^5. The PAPR of ACO-OFDM is nearly 3 dB higher than w/o clipping OFDM. This result is good agreement with the analysis in Section 3.1. When the DHT-spread technique is employed, the PAPR performance of ACO-OFDM is significantly improved. At the probability of 10^{-3}, PAPR has been decreased by about 9.7 dB when 2-PAM is modulated and about 6.2 dB when 4-PAM is modulated. The PAPR of DHT-S-ACO-OFDM is about 6 dB when 2-PAM is modulated, which is consistent with the theoretical derivation in (9).

3.3. BER Performance in AWGN Channel

Fig. 4 depicts BER performance of conventional ACO-OFDM and DHT-S-ACO-OFDM where N is 256 in additive white Gaussian noise (AWGN) channel. When the same simulation parameters are adopted, BER curves of DHT-S-ACO-OFDM coincide to those of conventional ACO-OFDM. We can draw a conclusion that the BER performance of DHT-S-ACO-OFDM is the

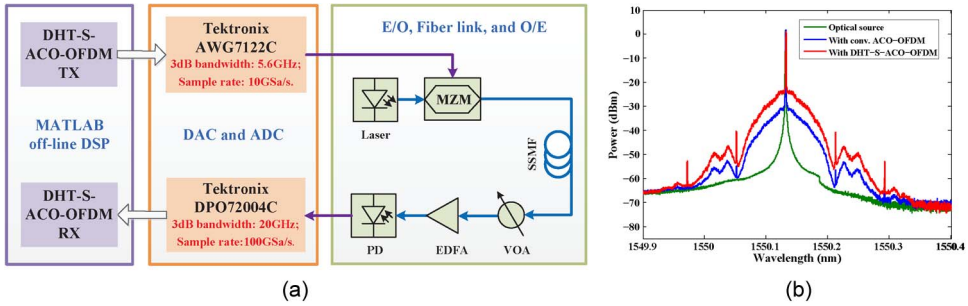

Fig. 5. (a) Experimental setup of DHT-S-ACO-OFDM. (b) Optical spectrum for DHT-S-ACO-OFDM and conventional ACO-OFDM.

same as that of conventional ACO-OFDM. The BER performance of DHT-S-ACO-OFDM is not influenced by DHT-spread operation in AWGN channel.

4. Experiment Setup and Results

4.1. Experiment Setup

Fig. 5(a) shows the experimental setup of DHT-S-ACO-OFDM. In our experiment, DHT-S-ACO-OFDM was encoded by MATLAB. 2-PAM signal was spread by 128-point DHT (i.e., $L = 128$). After spreading operation, OFDM signals can be obtained by 256-point DHT (i.e., $N = 256$). Sixteen cyclic prefix samples were employed. For every 128 symbols, 10 training symbols for channel estimation and one synchronization symbol were transmitted. The generated digital signal was then uploaded into an arbitrary waveform generator (Tektronix AWG7122C) operating at 10 GS/s to realize DAC. So the overall link rate was about 10 Gb/s. The net bit rate can be calculated by [19]

$$\begin{aligned}\text{Net bit rate} &= 1\ \text{bit/sample (2-PAM)} \times 10\ \text{GS/s (sampling rate)} \\ &\times \frac{128\ \text{(payload subcarriers)}}{256\ \text{(total subcarriers)} + 16\ \text{(cyclic prefix)}} \\ &\times \frac{128\ \text{(payload symbols)}}{128\ \text{(payload symbols)} + 10\ \text{(training symbols)} + 1\ \text{(sync. symbol)}} \\ &\approx 4.3\ \text{Gb/s.}\end{aligned} \tag{11}$$

A laser with 5-kHz line-width was used to generate the optical carrier. A Mach–Zehnder modulator (MZM) was adopted to modulate the optical carrier with the generated analog signal without DC bias. At the receiver, a variable optical attenuator (VOA) was used to vary the received optical power. We used an EDFA worked at power-controlled status to maintain a constant input power of photodiode (PD). The received optical signal can be converted into electrical signal by the PD. The electrical signal was then filtered by an LPF with a 3 dB bandwidth of 10 GHz. The filtered electrical signal was captured by a real-time digital phosphor oscilloscope (Tektronix DPO72004C, 100-GS/s sample rate, 20-GHz 3-dB bandwidth)) to implement ADC. The generated digital signal was decoded by off-line processing in MATLAB.

4.2. Experiment Results

Fig. 5(b) reveals the optical spectrum (1.12-pm resolution) of the optical carrier before and after modulated by conventional ACO-OFDM and DHT-S-ACO-OFDM with 2-PAM constellation. In our experiment, the encoding process of conventional ACO-OFDM was the same as the DHT-S-ACO-OFDM except was without DHT-spread operation. The launch power of the laser remained unchanged. The output signals of AWG7122C had the same sample rate. Meanwhile, they were normalized and fitted to DAC range. Under the same peak power, the average power of DHT-S-ACO-OFDM is larger than that of conventional ACO-OFDM due to its low PAPR.

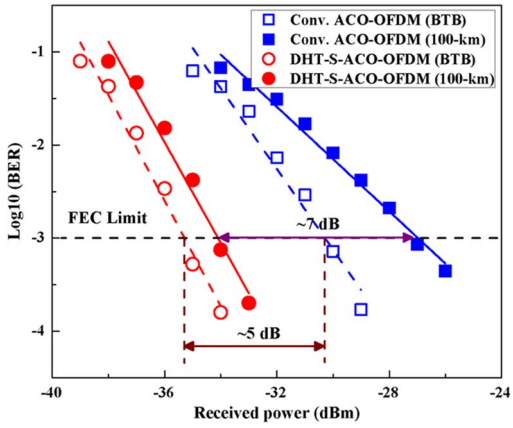

Fig. 6. BER curves for conventional ACO-OFDM and DHT-S-ACO-OFDM when 2-PAM is modulated.

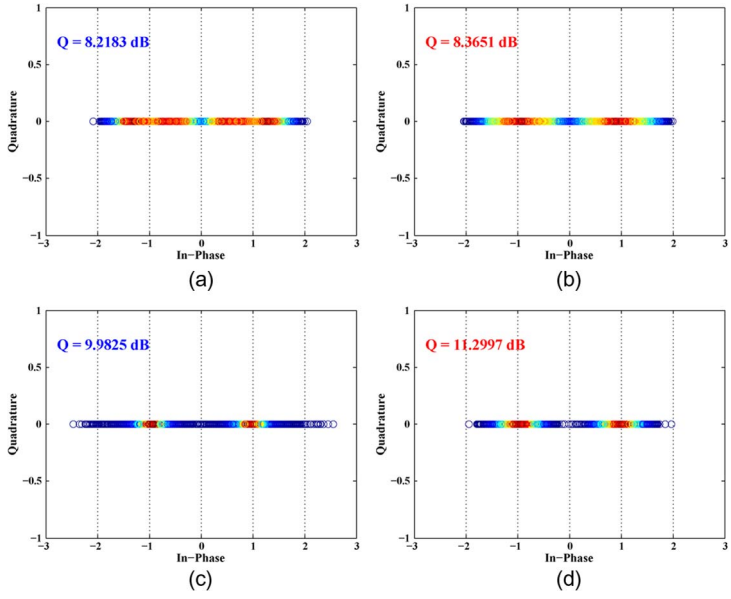

Fig. 7. Constellation diagrams of received signal after 100-km transmission. (a) Conventional ACO-OFDM without equalization; (b) DHT-S-ACO-OFDM without equalization; (c) conventional ACO-OFDM with equalization; (d) DHT-S-ACO-OFDM with equalization.

From Fig. 5(b) we can get that the optical signal-to-noise ratio (OSNR) of DHT-S-ACO-OFDM is higher than conventional ACO-OFDM.

Fig. 6 depicts the BERs versus received power for conventional ACO-OFDM and DHT-S-ACO-OFDM with 2-PAM constellation after back-to-back (BTB) and 100-km SSMF transmission. The optical signals with power of 3 dBm were injected into the 100-km SSMF. In DHT-S-ACO-OFDM system, the required received power at the FEC limit was measured to be about −35.3 dBm and −34 dBm for B2B and 100-km SSMF transmission, respectively. The maximum power penalty for the case of 100-km SSMF transmission was about 1.3 dB. In the case of BTB, DHT-S-ACO-OFDM had about 5 dB improvement of received sensitivity at FEC limit compared to conventional ACO-OFDM. After 100-km SSMF transmission, the improvement expanded to about 7 dB because conventional ACO-OFDM may suffer more fiber nonlinear distortions due to its high PAPR.

Fig. 7 shows the constellation diagrams of the received signal after 100-km SSMF transmission for (a) conventional ACO-OFDM without equalization, (b) DHT-S-ACO-OFDM without

equalization, (c) conventional ACO-OFDM with equalization, (d) DHT-S-ACO-OFDM with equalization. The same equalization was used in conventional ACO-OFDM and DHT-S-ACO-OFDM. Fig. 7(a) and (b) depict two constellation diagrams with almost the same Q factor before equalization for conventional ACO-OFDM and DHT-S-ACO-OFDM, respectively. The Q factor was obtained from the measured BER. After equalization, the Q factor for DHT-S-ACO-OFDM was about 11.3 dB and the Q factor for conventional ACO-OFDM was about 10 dB. The Q factor for DHT-S-ACO-OFDM was 1.3 dB larger than that for conventional ACO-OFDM. As shown in Fig. 7(c) and (d), the constellation diagram of DHT-S-ACO-OFDM is much clearer than that of the conventional ACO-OFDM.

5. Conclusion

In this paper, we propose a DHT-spread technique for PAPR reduction in DHT-based ACO-OFDM system. At the CCDF of 10^{-3}, the PAPR values of our proposed scheme are about 9.7 dB and 6.2 dB lower than those of conventional ACO-OFDM for 2-PAM and 4-PAM, respectively. The transmission experiment over 100-km SSMF had been realized to verify the feasibility of the proposed scheme. In our experiment, the proposed scheme had an about 7-dB improvement of received sensitivity at FEC limit compared to conventional scheme. The proposed scheme has better transmission performance than the conventional scheme due to its effective equalization and low PAPR. In conclusion, the proposed scheme is attractive to IM/DD systems due to its low PAPR and excellent transmission performance.

References

[1] W. Shieh, H. Bao, and Y. Tang, "Coherent optical OFDM: Theory and design," *Opt. Exp.*, vol. 16, no. 2, pp. 841–859, 2008.
[2] J. Armstrong, "OFDM for optical communications," *J. Lightw. Technol.*, vol. 27, no. 3, pp. 189–204, Feb. 2009.
[3] X. Liu *et al.,* "448-Gb/s reduced-guard-interval CO-OFDM transmission over 2000 km of ultra-large-area fiber and five 80-GHz-grid ROADMs," *J. Lightw. Technol.*, vol. 29, no. 4, pp. 483–490, Feb. 2011.
[4] O. Gonzalez, R. Perez-Jimenez, S. Rodriguez, J. Rabadan, and A. Ayala, "OFDM over indoor wireless optical channel," *Proc. Inst. Elect. Eng.—Optoelectron.*, vol. 152, no. 4, pp. 199–204, Aug. 2005.
[5] A. M. Khalid, G. Cossu, R. Corsini, P. Choudhury, and E. Ciaramella "1-Gb/s transmission over a phosphorescent white LED by using rate-adaptive discrete multitone modulation," *IEEE Photon. J.*, vol. 4, no. 5, pp. 1465–1473, Oct. 2012.
[6] P. Cao *et al.,* "Physical layer encryption in OFDM-PON employing time-variable keys from ONUs," *IEEE Photon. J.*, vol. 6, no. 2, pp. 1–6, Apr. 2014.
[7] J. Armstrong and A. J. Lowery, "Power efficient optical OFDM," *Electron. Lett.*, vol. 42, no. 6, pp. 370–372, Mar. 2006
[8] J. Armstrong and B. Schmidt, "Comparison of asymmetrically clipped optical OFDM and DC-biased optical OFDM in AWGN," *Commun. Lett.*, vol. 12, no. 5, pp. 343–345, May 2008.
[9] L. Chen, J. Zhou, Y. Qiao, Z. Huang, and Y. Ji, "Novel modulation scheme based on asymmetrically clipped optical orthogonal frequency division multiplexing for next-generation passive optical networks," *J. Opt. Commun. Netw.*, vol. 5, no. 8, pp. 881–887, Aug. 2013.
[10] S. D. Dissanayake and J. Armstrong, "Comparison of ACO-OFDM, DCO-OFDM and ADO-OFDM in IM/DD systems," *J. Lightw. Technol.*, vol. 31, no. 7, pp. 1063–1072, Apr. 2013.
[11] M. S. Moreolo, R. Munoz, and G. Junyent, "Novel power efficient optical OFDM based on Hartley transform for intensity-modulated direct-detection systems," *J. Lightw. Technol.*, vol. 28, no. 5, pp. 798–805, Mar. 2010.
[12] J. Zhou, Y. Yan, Z. Cai, Y. Qiao, and Y. Ji, "A cost-Effective and efficient scheme for optical OFDM in short-range IM/DD systems," *IEEE Photon. Technol. Lett.*, vol. 26, no. 13, pp. 1372–1374, Jul. 2014.
[13] R. N. Bracewell, "Discrete Hartley transform," *J. Opt. Soc. Amer.*, vol. 73, no. 12, pp. 1832–1835, 1983.
[14] F. Li, X. Li, J. Yu, and L. Chen, "Optimization of training sequence for DFT-spread DMT signal in optical access network with direct detection utilizing DML," *Opt. Exp.*, vol. 22, no. 19, pp. 22962–22967, Sep. 2014.
[15] Y. Tang, W. Shieh, and B. S. Krongold, "DFT-spread OFDM for fiber nonlinearity mitigation," *IEEE Photon. Technol. Lett.*, vol. 22, no. 16, pp. 1250–1252, Aug. 2010.
[16] X. Chen, A. Li, G. Gao, and W. Shieh, "Experimental demonstration of improved fiber nonlinearity tolerance for unique-word DFT-spread OFDM systems," *Opt. Exp.*, vol. 19, no. 27, pp. 26198–26207, Dec. 2011.
[17] M. Sung, S. Kang, J. Shim, J. Lee, and J. Jeong, "DFT-precoded coherent optical OFDM with Hermitian symmetry for fiber nonlinearity mitigation," *J. Lightw. Technol.*, vol. 30, no. 17, pp. 2757–2763, Sep. 2012.
[18] D. Lim, J. No, C. Lim, and H. Chung, "A new SLM OFDM scheme with low complexity for PAPR reduction," *IEEE Signal Process. Let.*, vol. 12, no. 2, pp. 93–96, Feb. 2005.
[19] Q. Yang *et al., "Coherent optical DFT-spread OFDM transmission using orthogonal band multiplexing," Opt. Exp.*, vol. 20, no. 3, pp. 2379–2385, 2012.